npj | climate and atmospheric science

www.nature.com/npjclimatsci

ARTICLE OPEN

Check for updates

A diurnal story of $\Delta^{17}O(NO_3^-)$ in urban Nanjing and its implication for nitrate aerosol formation

Yan-Lin Zhang[1,2,3]✉, Wenqi Zhang[1,2,3,4], Mei-Yi Fan[1,2,3], Jianghanyang Li[5], Huan Fang[5], Fang Cao[1,2,3], Yu-Chi Lin[1,2,3], Benjamin Paul Wilkins[5], Xiaoyan Liu[1,2,3], Mengying Bao[1,2,3], Yihang Hong[1,2,3] and Greg Michalski[5]

Inorganic nitrate production is critical in atmospheric chemistry that reflects the oxidation capacity and the acidity of the atmosphere. Here we use the oxygen anomaly of nitrate ($\Delta^{17}O(NO_3^-)$) in high-time-resolved (3 h) aerosols to explore the chemical mechanisms of nitrate evolution in fine particles during the winter in Nanjing, a megacity of China. The continuous $\Delta^{17}O(NO_3^-)$ observation suggested the dominance of nocturnal chemistry ($NO_3 + HC/H_2O$ and $N_2O_5 + H_2O/Cl^-$) in nitrate formation in the wintertime. Significant diurnal variations of nitrate formation pathways were found. The contribution of nocturnal chemistry increased at night and peaked (72%) at midnight. Particularly, nocturnal pathways became more important for the formation of nitrate in the process of air pollution aggravation. In contrast, the contribution of daytime chemistry ($NO_2 + OH/H_2O$) increased with the sunrise and showed a highest fraction (48%) around noon. The hydrolysis of N_2O_5 on particle surfaces played an important role in the daytime nitrate production on haze days. In addition, the reaction of NO_2 with OH radicals was found to dominate the nitrate production after nitrate chemistry was reset by the precipitation events. These results suggest the importance of high-time-resolved observations of $\Delta^{17}O(NO_3^-)$ for exploring dynamic variations in reactive nitrogen chemistry.

npj Climate and Atmospheric Science (2022)5:50 ; https://doi.org/10.1038/s41612-022-00273-3

INTRODUCTION

Nitrate (NO_3^-) and its precursor NO*x* (NO*x* = NO + NO_2) play a crucial role in atmospheric chemical processes and the formation of $PM_{2.5}$, fine particles with diameter less than 2.5 μm[1,2]. Tropospheric NO*x* oxidation drives the formation of ozone (O_3) and recycle of hydroxyl radicals (OH) that control the atmospheric self-cleansing capacity[3]. Majority of NO*x* emitted from various sources are finally converted into nitric acid (HNO_3) and organic nitrate (e.g., $RONO_2$) through atmospheric oxidation processes by oxidants (e.g., O_3, OH, HO_2, and RO_2)[4]. HNO_3 lowers the pH of the precipitation and increases the risk of forming acid rain[5]. Furthermore, HNO_3 easily be transformed into nitrate particles through atmospheric reactions with alkaline ammonia that in turn influence the chemical composition and the size of existing particles, affecting the formation of clouds and precipitation as well[3,6]. $RONO_2$ can partition into the particle phase ($RONO_{2(p)}$) and then is removed from the atmosphere by deposition to the surface or through hydrolysis to form inorganic nitrate and alcohols[7,8]. Atmospheric nitrate in gas phase ($HNO_{3(g)}$), liquid phase ($HNO_{3(aq)}$) and particulates ($NO_{3\,(p)}^-$) are eventually removed through wet/dry deposition. Thus investigating the mechanism of NO*x*-NO_3^- conversion is important to the study of atmospheric chemistry.

The conversion of NO*x* to NO_3^- is a combination of the NO*x* cycle (Supplementary Note 1) and nitrate production processes. During the day, OH radical is easily generated under the strong sunlight and $HNO_{3(g)}$ is then formed through the $NO_2 + OH$ reaction[9]. NO_2 can be hydrolyzed on surfaces to produce $HNO_{3(aq)}$[10], which was found to be a weak source of nitrate formation on severe haze days in winter in the North China Plain (NCP)[11,12]. In addition, NO_2 can also react with O_3 to form NO_3 radicals and then NO_3 directly reacts with hydrocarbon (HC) and dimethylsulfide (DMS) or be hydrolyzed on surfaces to produce HNO_3[13–15]. This reaction occurred at night because NO_3 radical is easily photolyzed to NO_2 under sunlight[16]. And the contribution of $NO_3 + DMS$ is small in non-coastal areas due to the low mixing ratio of DMS[17]. Dinitrogen pentoxide (N_2O_5), a nocturnal NO*x* reservoir, can react on airborne particle surface to produce only $HNO_{3(aq)}$ or both $NO_{3\,(p)}^-$ and nitryl chloride ($ClNO_2$)[18]. Other potential formation mechanisms of nitrate particles, like the hydrolysis of organic nitrates ($RONO_2$) and halogen nitrates (XNO_3), might be important in coastal regions or the rainforest areas like Amazonia[13].

$$NO_2 + OH + M \rightarrow HNO_3 + M \quad (1)$$

$$2NO_2 + H_2O(surface) \rightarrow HNO_3(liquid) + HONO \quad (2)$$

$$NO_2 + O_3 \rightarrow NO_3 + O_2 \quad (3)$$

$$NO_3 + HC/DMS \rightarrow HNO_3 + Others \quad (4)$$

$$NO_3 + H_2O(surface) \rightarrow HNO_3(liquid) + OH \quad (5)$$

$$NO_2 + NO_3 \leftrightarrow N_2O_5 \quad (6)$$

$$N_2O_5 + H_2O(surface) \rightarrow 2HNO_3(liquid) \quad (7)$$

$$N_2O_5 + Cl^-(surface) \rightarrow NO_3^-(particle) + ClNO_2 \quad (8)$$

[1]Atmospheric Environment Center, International Joint Laboratory on Climate and Environment Change (ILCEC), Nanjing University of Information Science & Technology, Nanjing 210044, China. [2]School of Applied Meteorology, Nanjing University of Information Science & Technology, Nanjing 210044, China. [3]Key Laboratory of Meteorological Disaster, Ministry of Education (KLME)/Collaborative Innovation Center on Forecast and Evaluation of Meteorological Disasters (CIC-FEMD), Nanjing University of Information Science & Technology, Nanjing 210044, China. [4]Ningbo Meteorological Bureau of Zhejiang Province, Ningbo 315012, China. [5]Department of Earth, Atmospheric and Planetary Sciences and Department of Chemistry, Purdue University, 550 Stadium Mall Drive, West Lafayette, IN 47907, USA. ✉email: zhangyanlin@nuist.edu.cn

In the past, $NO_2 + OH$ photochemical reaction and N_2O_5 hydrolysis have been widely considered as the main pathways of nitrate formation worldwide[13,19]. However, $NO_3 + HC$ reaction was reported to be an important pathway for nitrate formation in industrial regions due to the extensive emissions of hydrocarbons (HCs) from anthropogenic sources[14]. Previous studies suggested that N_2O_5 uptake in aerosols and clouds was the dominant nitrate production pathway during intense haze events under low temperatures and minimal sunlight conditions[20,21]. Some laboratory studies suggested that the hydrolysis of NO_2 and NO_3 was not important for HNO_3 formation because of its low reaction probability[22–24]. A recent model simulation found that NO_2 hydrolysis was a neglected source of nitrate formation on haze days in Beijing winter[11]. And the heterogeneous reactions of NO_3 and N_2O_5 on the aerosol surface have been pointed out to dominate the particulate nitrate formation on polluted days in urban Shanghai based on the high-time resolution observation[25]. Platt et al.[26] also pointed out that the lifetimes for NO_3 radicals were shorter than 1 min in the presence of fog, which indicated a fast reaction of N_2O_5 or NO_3 with liquid water droplets.

Triple oxygen isotope (^{16}O, ^{17}O, and ^{18}O) analysis of atmospheric nitrate is a powerful technique used to identify nitrate formation pathways[19,27]. The only exception to the mass-dependent oxygen isotope fractionation rule ($\delta^{17}O = 0.52 \times \delta^{18}O$)[28] occurs during O_3 production (heavy oxygen isotopes are equally enriched). This isotope fractionation that appears independent of relative mass differences is termed as mass-independent fractionation and is quantified by $\Delta^{17}O = \delta^{17}O - 0.52 \times \delta^{18}O$[29]. The $\Delta^{17}O$ signature of O_3 is transferred through oxidation reactions to other oxygen-bearing compounds (e.g., NO_2, NO_3, and N_2O_5) and the $\Delta^{17}O$ of these atmospheric species acts as a marker of the influence of O_3 in their chemical formation. $\Delta^{17}O$ of atmospheric nitrate (the $\Delta^{17}O$ of compound X is expressed as $\Delta^{17}O(X)$ in this paper. $\Delta^{17}O(NO_3^-)$ normally shows positive values from 12 to 43‰[30] due to the oxygen atom transfer from O_3 to NO_3^- during the NOx oxidation. Moore and Semmens[31] reported a large range of $\Delta^{17}O(O_3)$ (20–40‰). Modeling studies that seek to simulate the propagation of $\Delta^{17}O$ in the atmosphere typically assume a $\Delta^{17}O(O_3)$ value of 25–35‰[19]. However, the $\Delta^{17}O$ of tropospheric O_3 has been observed to average at 26 ± 1‰[32,33]. Except for O_3, the $\Delta^{17}O$ values of all the oxygen atoms that may be incorporated into nitrate (i.e., water vapor, OH radical, and HO_2 (ROx)) are close to 0‰[34–39]. Thus $\Delta^{17}O(NO_3^-)$ actually reflects the fraction of O_3 derived oxygen atoms incorporated into NO_3^-, which varies depending on the nitrate formation pathways. In recent years, the use of $\Delta^{17}O(NO_3^-)$ in revealing reactive nitrogen chemistry in China has gotten considerable attention. He et al.[20] found that nocturnal reactions (including $NO_3 + HC$ and N_2O_5 uptake) dominated nitrate formation along with high ambient humidity and weak sunlight during polluted days in Beijing. Fan et al.[40] suggested nocturnal chemistry contributed to nitrate production equally with $NO_2 + OH/H_2O$ at ground level, but dominated the nitrate production in the air aloft (260 m) under higher O_3 and aerosol liquid water content (ALWC) conditions based on tower observation. The average fractions of $NO_2 + OH$ and N_2O_5 hydrolysis were estimated to be 43 and 52% of nitrate production over the Himalayan-Tibetan Plateau[41].

Although many modeling and observation studies focused on the variation of nitrate production influenced by factors such as clean versus haze days[11,42,43], it's necessary to explore the diurnal variation of nitrate production pathways which can provide us new insights into the dynamic variations in nitrate chemistry. Many field measurements showed large differences in oxidants (e.g., O_3, OH, and HO_2)[44,45] and meteorology (e.g., solar radiation and boundary layer height)[46,47] between daytime and nighttime in urban areas, which probably caused the different nitrate chemical processes at different times of the day. Huang et al.[48] found that the aqueous-phase processes played an important role in nitrate production during the nighttime in the NCP. Kuang et al.[49] suggested that the prevailing NH_3 morning spikes on the NCP significantly influenced nitrate formation and atmospheric chemistry. Tan et al.[50] highlighted that the HNO_3 production was less efficient throughout the boundary layer than that was observed in the surface layer. Liu et al.[51] found that $NO_2 + OH$ reaction played a pivotal role in the daytime formation of nitrate at moderate relative humidity (RH). However, this is a lack of investigation of the diurnal variations of nitrate formation mechanisms based on the multiple oxygen isotopes observations, which can further provide direct evidence to understand the dynamic nitrate chemistry in the real atmosphere.

In this study, $\Delta^{17}O(NO_3^-)$ measurements were conducted in high-time-resolved winter aerosols collected during a haze event in Nanjing, a megacity in eastern China. The contribution of each nitrate formation pathway was evaluated based on the combination of $\Delta^{17}O(NO_3^-)$ observations and the Bayesian model. The diurnal variations of nitrate production pathways were assessed and the differences between these pathways during clean and haze days were also explained.

RESULTS AND DISCUSSION

Temporal variation of chemical species, meteorological conditions, and $\Delta^{17}O$ of nitrate

The $PM_{2.5}$ mass concentrations ranged from 19.3 to 263.7 μg m^{-3} with an average value of 105.4 ± 61.7 μg m^{-3} (Fig. 1a). The mass concentration of nitrate varied from 3.3 to 68.7 μg m^{-3} (Fig. 2a). The first few sampling days (January 14th 2:00 to 16th 8:00) were classified as "clean days" based on low $PM_{2.5}$ levels (39.0 ± 13.6 μg m^{-3}). After January 21st 8:00, $PM_{2.5}$ showed consecutively high values (> 75 μg m^{-3}) and increased up to 271.7 μg·m^{-3} on January 25th. Time period from January 21st 8:00 to 27th 2:00 was defined as a haze period ($PM_{2.5}$ > 75 μg m^{-3}) according to the Grade II of NAAQS (National Ambient Air Quality Standard) in China. The severe haze ended when the majority of $PM_{2.5}$ was scavenged by the precipitation on January 27th. Visibility was relatively high (4.0 ± 0.7 km) during the clean days and extremely low (≈1 km) during the most severe haze period (January 24th to 26th) (Fig. 1a). Three precipitation events (less than 4 mm for each) were observed on January 14th, 25th, and 27th, resulting in the decrease of $PM_{2.5}$ levels with fractions of 52–82% (Fig. 1a). Air temperature varied from −1.1 to 12.8 °C and was negatively correlated ($r = -0.56$, $p < 0.001$) with RH, which ranged from 19 to 84% (Fig. 1b). The wind speed was less than 3.7 m·s^{-1} and was either from the north or east to south (Fig. 1c). RH was used to estimate the trend of planetary boundary layer height (PBLH) using the Clausius–Claperyron Equation (Supplementary Note 2). The obtained PBLH was higher in the daytime (865 ± 528 m) and lower at night (770 ± 458 m) (Fig. 2d).

The mixing ratio of O_3 ranged from 0.5 to 37.3 ppb and was higher during the day compared to the night (Fig. 2b). The extremely low O_3 concentrations (<10 ppb) were observed in the most severe haze period (January 24th to 26th). NO_2 concentrations ranged from 6.9 to 84.3 ppb with an average value of 28.2 ± 17.4 ppb and CO concentrations varied from 0.1 to 2.2 ppm (Fig. 2c). The NO_3^- mass concentration was correlated with both CO ($r = 0.87$, $p < 0.01$) and NO_2 ($r = 0.72$, $p < 0.01$) during the sampling period. Nitrogen oxidation ratio (NOR = $[NO_3^-]/([NOx] + [NO_3^-])$, a proxy for the secondary formation of nitrate[52]) varied between 0.08 and 0.54 without significant diurnal variation. $\Delta^{17}O(NO_3^-)$ ranged from 23.4 to 39.3‰ (Fig. 2a), with a weighted average value of 30.5‰. These values are within the range of most previous observations (12–43‰)[30,43,53]. Especially, the $\Delta^{17}O(NO_3^-)$ values in $PM_{2.5}$ in this study were similar with those observed during winter in Beijing (30.6 ± 1.8‰)[20] and Shanghai (20.5–31.9‰)[54], but higher than those in winter in Taiwan

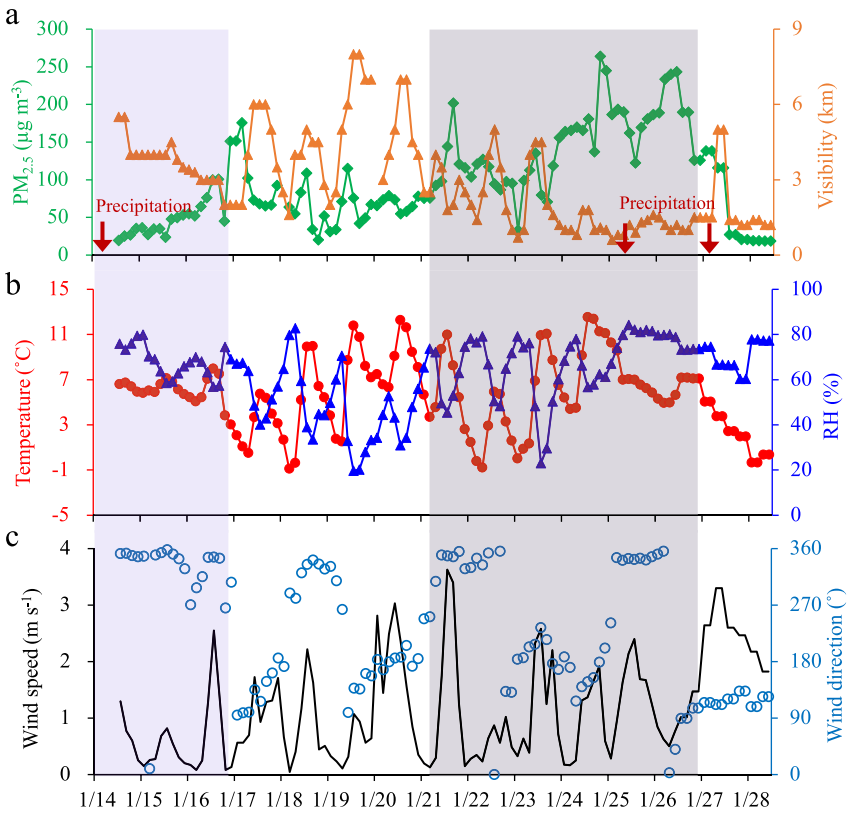

Fig. 1 Evolution of meteorological parameters and particle mass concentration during the haze event. Time series of **a** mass concentrations of fine particulate matter ($PM_{2.5}$, green line) and visibility (orange line), **b** temperature (red line) and relative humidity (blue line), **c** wind speed (black line) and wind direction (dark blue circle) during the haze event from January 14th to January 28th, 2015. The blue rectangle represents clean period and the gray rectangle represents haze period.

province (23 ± 5‰)[53]. In this work, $\Delta^{17}O(NO_3^-)$ were similar during clean (24.0–34.4‰) and haze days (23.4–33.6‰).

Contrary to most investigating days, extremely high $\Delta^{17}O(NO_3^-)$ at noon were observed on January 17th, 18th, 19th, and 27th (Fig. 2a). In the case on January 17th, the nitrate aerosols possessed a $\Delta^{17}O$ value of 39.3‰, which exceeded the terminal value of O_3 (~39‰) produced in the troposphere (Eq. (17)). This suggests that the tropospheric produced NO_3^- could not completely explain this enhanced $\Delta^{17}O(NO_3^-)$ value. Previously, such high $\Delta^{17}O(NO_3^-)$ values have been found in polar areas and high-altitude localities like Nepal Climate Observatory-Pyramid (5079 m a.s.l.), where the stratospheric intrusion of O_3 and nitrate with high $\Delta^{17}O$ values frequently occurred in winter and spring seasons[38,41,55–58]. Thus, the high $\Delta^{17}O(NO_3^-)$ value on January 17th might be attributed to a mixed source from the tropospheric and stratospheric intrusion of O_3 and nitrate. In urban areas, the daily $\Delta^{17}O(NO_3^-)$ has been observed more than 35‰ in the polluted upper air (260 m a.s.l.) in Beijing winter[40]. There were other possible explanations for the high $\Delta^{17}O(NO_3^-)$ values around noontime: the oxidation pathways of HNO_3 during the current period and the external input of nitrate through vertical/horizontal air mass transport. The variation of PBLH was similar on January 17th, 18th, and 19th; PBLH was lower (~500 m) at night and increased to higher values (1500–2500 m) at noon. During the nighttime, large anthropogenic-emitted pollutants (e.g., NO*x*, VOCs, CO) reached above the top of the nocturnal boundary layer and nitrate was produced in the residual layer without sinking[59–61]. Then, the increased PBLH during the day promoted the mixture of materials in the boundary layer at noon, allowing nitrate transport from the top of the PBLH to the surface layer (Supplementary Fig. 1). This suggested the high $\Delta^{17}O(NO_3^-)$ might be related to vertical air mass transport. Vertical air mass transport increased the fraction of nitrate produced above the boundary layer at night and decreased the contribution of nitrate produced in the surface layer during the day. In that case, the nitrate produced at night (such as through NO_3 + HC pathway) with high $\Delta^{17}O(NO_3^-)$ was collected at noon. In particular, a high concentration of Ca^{2+} was found with the increase of PBLH on January 19th (Supplementary Fig. 2). The footprints of nitrate aerosols at noon on January 19th from the FLEXPART model (Supplementary Note 3 and Supplementary Fig. 3) suggested that the dust air was affected by air mass transport from southeast of the sampling site where some chemical industries and steel plants located and nitrate particles might be formed in the process of region transport. On the contrary, the PBLH was relatively low (~400–700 m) on January 27th, but the high wind speed (3.3 m s^{-1}) at noon might also bring the nitrate with a high $\Delta^{17}O$ value from northeast to the sampling site. Without considering the four abnormal days with extremely high values of $\Delta^{17}O(NO_3^-)$ around noontime, the $\Delta^{17}O(NO_3^-)$ values at night (17:00–5:00 on the next day, 31.0 ± 2.6‰) were significantly higher (p-value = 0.002, Supplementary Table 1) than those during the day (5:00–17:30, 29.3 ± 3.0‰). This suggested the differences in relative contributions of photochemical and nocturnal reactions to nitrate formation during the day and night. In addition, nitrate concentration and $\Delta^{17}O(NO_3^-)$ decreased significantly after the three precipitation events on January 14th, 25th, and 27th in this study, suggesting the important role of reaction with depleted $\Delta^{17}O$ signature on the formation of nitrate after air cleaning by wet deposition.

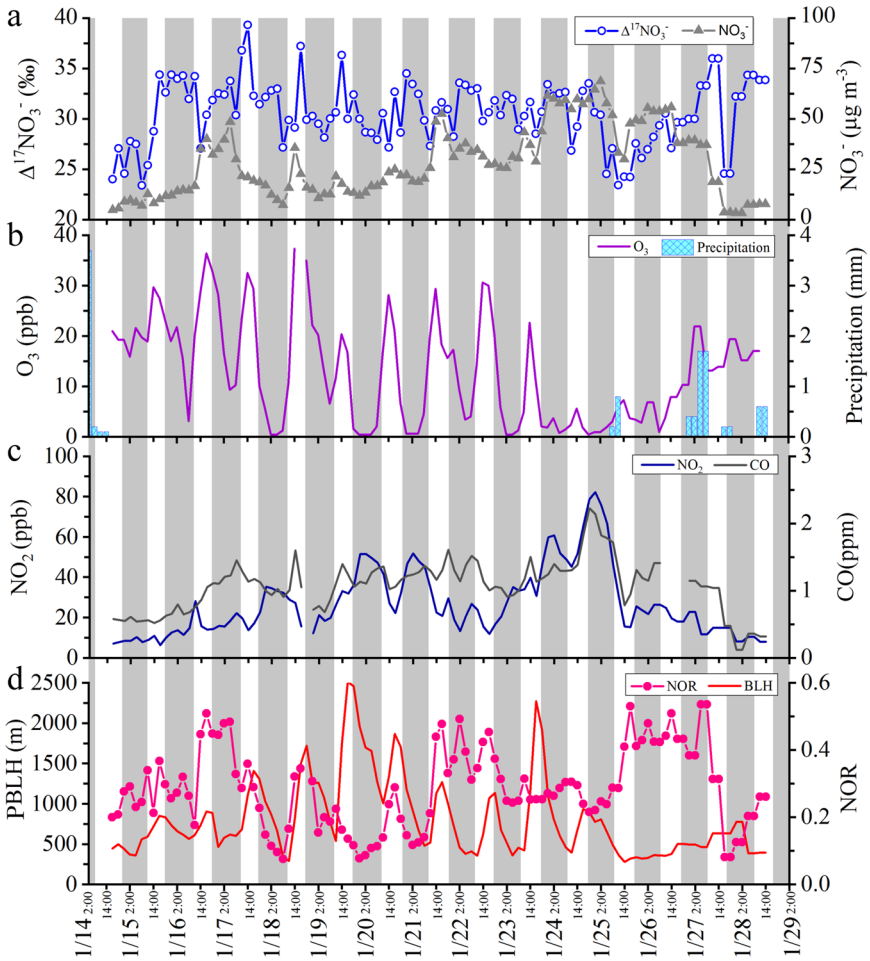

Fig. 2 Evolution of nitrate and its oxygen isotope anomaly during the haze event. Time series of **a** mass concentrations of nitrate (NO_3^-) aerosols and oxygen isotope anomaly of nitrate ($\Delta^{17}O(NO_3^-)$), **b** mass concentrations of ozone (O_3) and the precipitation, **c** mass concentrations of nitrogen dioxide (NO_2) and carbon monoxide (CO), **d** planetary boundary layer height (PBLH) and NO_2 oxidation ratio (NOR) during the haze event from January 14th to January 28th, 2015.

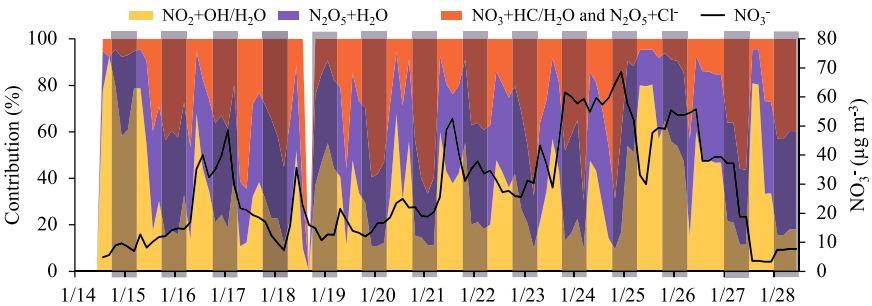

Fig. 3 Nitrate formation pathways during the haze event. Time series of mass concentrations of nitrate (NO_3^-, black line) and the relative contributions of three pathways (pathway 1: the reactions of nitrogen dioxide with hydroxyl radical and liquid water ($NO_2 + OH/H_2O$), pathway 2: the hydrolysis of nitrogen pentoxide ($N_2O_5 + H_2O$) and pathway 3: the reactions of nitrate radical with hydrocarbon and liquid water as well as the reaction of nitrogen pentoxide with chloridion on particle surface ($NO_3 + HC/H_2O$ and $N_2O_5 + Cl^-$)) to nitrate production during the haze event from January 14th to January 28th, 2015. The contribution fractions are estimated by the Bayesian model. The gray shades represent the night.

The diurnal variation of nitrate production

Observations of $\Delta^{17}O(NO_3^-)$ and estimated α were applied to quantify the contribution of each nitrate formation pathway using the Bayesian model. The α values ranged from 0.61 to 0.97 with higher values during the day (0.95 ± 0.04) and lower values at night (0.87 ± 0.11) (Supplementary Fig. 4), suggesting the significance of O_3 participation in NO oxidation during the sampling period. On the other hand, our α values were similar to those (0.85–1) for other midlatitude regions[19]. The α value is affected by the relative amount of O_3 and HO_2/RO_2 in NO*x* cycling. And the low O_3 concentrations (<1 ppb) were found when the α values were at a low level (~0.6) (Supplementary Fig. 4). The relative contributions of (P1: $NO_2 + OH/H_2O$, f_{P1}), (P2: $NO_3 + HC/H_2O$ and $N_2O_5 + Cl^-$, f_{P2}), and (P3: $N_2O_5 + H_2O$, f_{P3}) to diurnal nitrate

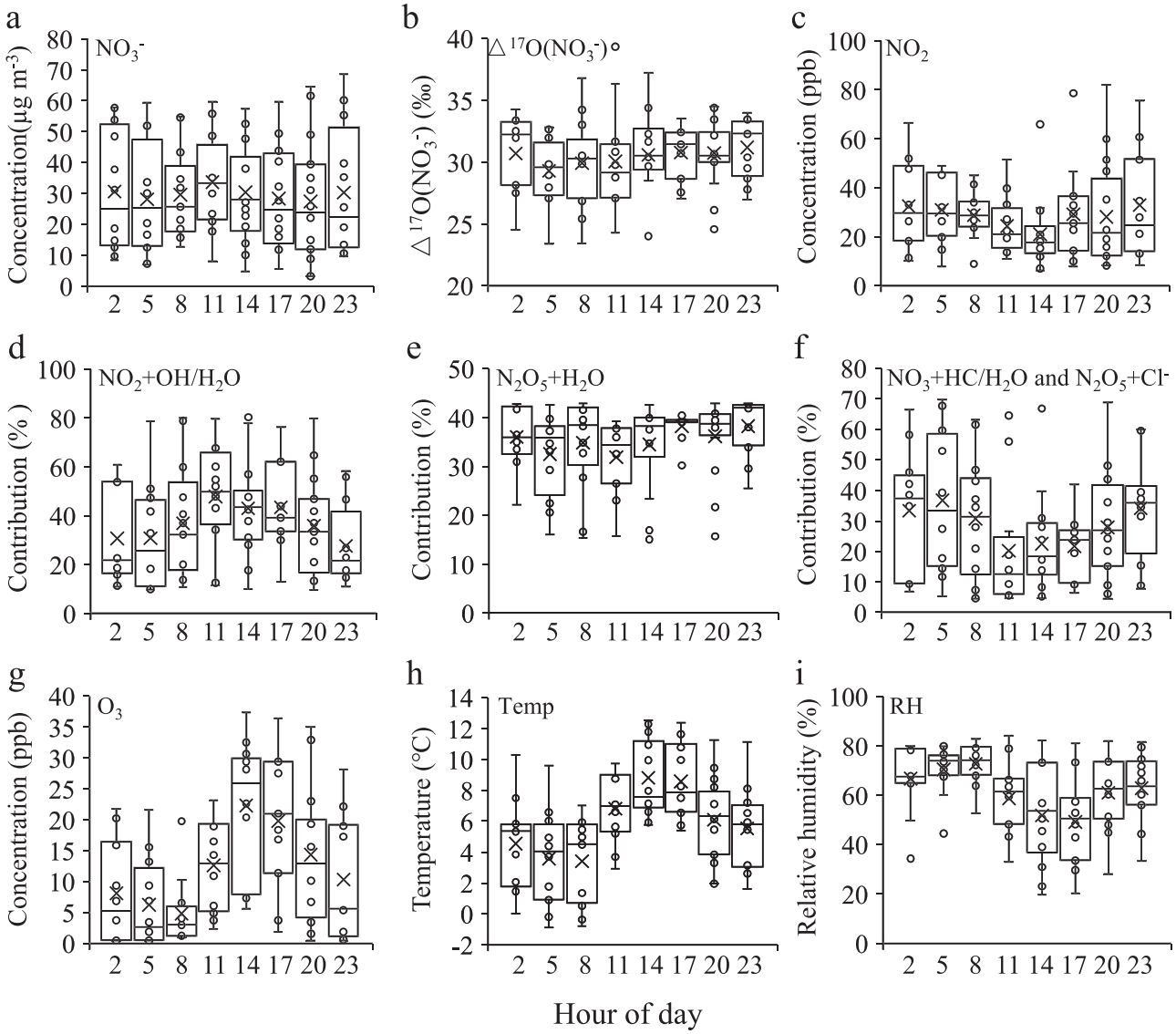

Fig. 4 Diurnal variations of nitrate formation pathways. The changes in **a** mass concentrations of nitrate (NO_3^-), **b** oxygen isotope anomaly of nitrate ($\Delta^{17}O(NO_3^-)$), **c** mass concentrations of nitrogen dioxide (NO_2), **d**–**f** the relative contributions of three pathways (pathway 1: $NO_2 + OH/H_2O$, pathway 2: $N_2O_5 + H_2O$ and pathway 3: $NO_3 + HC/H_2O$ and $N_2O_5 + Cl^-$) to nitrate production, **g** mass concentrations of ozone (O_3), **h** ambient temperature (temp) and **i** relative humidity (RH) throughout the day during the sampling period. The mean (cross), median (horizontal line), 25th and 75th percentiles (lower and upper box), and 10th and 90th percentiles (lower and upper whiskers) are shown in each box.

formation in Nanjing city are showed in Fig. 3 and Supplementary Fig. 5. On average, the f_{P1}, f_{P2}, and f_{P3} were 38 ± 10%, 27 ± 10%, and 35 ± 20% during the sampling period, which indicated the dominant role of nocturnal chemistry in nitrate formation during the winter in Nanjing. Our result was similar to the previous results in Beijing winter[40]. The average contributions of P1, P2, and P3 were 44 ± 21, 22 ± 16, and 34 ± 10% during the day, and 39 ± 19, 25 ± 17, and 36 ± 7% at night, respectively.

Significant diurnal variations of nitrate formation mechanisms were observed in this work (Fig. 4). The $NO_2 + OH/H_2O$ fraction increased to the highest (48 ± 20%) around noon (11:00–14:00) and decreased to the lowest (28 ± 16%) at midnight (23:00–2:00). The significant increase in the $NO_2 + OH/H_2O$ fraction during the day was predictable due to the diurnal pattern of OH radical concentration observed in previous studies[62,63]. The diurnal variation of ambient RH was contrary to the $NO_2 + OH/H_2O$ fraction, suggesting that NO_2 hydrolysis was not an essential reaction for the formation of nitrate in this work. In contrast, the increases in the relative fractions of the P2 and P3 pathways were observed at night, which peaked (34 ± 16% for P2 and 38 ± 6% for P3) at midnight and decreased to the lowest (20 ± 19% for P2 and 32 ± 7% for P3) at noon. As the precursors of NO_3 and N_2O_5, NO_2 and O_3 showed different diurnal patterns (Fig. 4). The NO_2 concentration levels were higher at night than during the day. In this case, the enriched NO_2 atmosphere and dark environment were responsible for generating NO_3 and N_2O_5 at night without being photolysis[62,64]. This has been proved by some previous studies[65,66]. A recent observational study in Nanjing found that the high level of volatile organic components (VOCs) concentrations in January 2015, which were emitted by various industrial sources nearby[67]. Thus, the active $NO_3 + HC$ reaction was considered as an important formation mechanism of particulate nitrate in Nanjing, especially at night. At the same time, peroxyl radicals (HO_2/RO_2) can be produced from the reaction of NO_3 with hydrocarbons. A previous study suggested the reaction rate of NO_3 radical with selected hydrocarbons (e.g., isobutene and trans-

2-butene) at night was slightly higher than that during the day in the winter[68]. However, the reaction of O_3 with hydrocarbons can also produce peroxyl radicals and the daytime reaction rate of O_3 with hydrocarbons was much higher than the nighttime reaction rate[68]. As shown in Fig. 4, O_3 concentrations during the day were much higher than those at night. This would cause the nighttime HO_2/RO_2 production to be much lower than the daytime production of HO_2/RO_2, which has been proved in many previous studies[69,70]. Besides, the higher RH values at night could facilitate the nitrate formation through heterogeneous processes (e.g., NO_3 hydrolysis and N_2O_5 uptake)[71]. Consequently, our results suggested that the nocturnal chemistry (including $NO_3 + HC/H_2O$ and $N_2O_5 + Cl^-/H_2O$) dominated the nitrate formation at night, while the $NO_2 + OH/H_2O$ pathway and nocturnal reactions contributed equally to nitrate production during the day in this study.

In this work, both daytime and nocturnal chemistry contributed to nitrate formation at different times of the day. Daytime NO_3 and N_2O_5 chemistry is generally regarded as less important due to rapid NO_3 photolysis and the titration reaction initiated by NO. A previous study showed that there was also a certain amount of NO_3 radical during the day compared with the night in cold seasons due to the weak sunlight[65]. The daytime production rate of NO_3 was found to be large because of the elevated NO_2 and O_3 concentrations in Taizhou of the Yangzi River Plain[72]. The N_2O_5 and NO_3 concentrations are very low during the daytime, however, both species exhibited non-neglected (even high) concentrations in urban cities, especially during the PM haze events. This resulted in high contributions of nocturnal mechanisms to nitrate formation during the day[73]. In addition, the global lifetime of atmospheric inorganic nitrate is on the order of 3–4 d[74], both the accumulated nitrate (i.e., the old nitrate produced prior to the current sampling period) and fresh nitrate (i.e., the new nitrate produced during the current sampling period) were collected in the high-time-resolved (3 h) samples and had impacts on $\Delta^{17}O(NO_3^-)$. This meant that the $\Delta^{17}O(NO_3^-)$ collected at noon was influenced by the nitrate production pathways of fresh nitrate and the nitrate generated during the previous night. On the other hand, the variation of NO_2 formation mechanism also had impacts on $\Delta^{17}O(NO_3^-)$ and then the estimated results[75]. During the day, a large quantity of NO_2 was produced through the NO*x* cycle and had $\Delta^{17}O(NO_2) = a\Delta^{17}O(O_3^*)$[19]. After sunset, NO_2 was mainly produced with the absence of NO_2 photolysis and the NO*x* cycle was not able to complete. Only half of the oxygen atoms in each NO_2 molecule was oxidized by O_3 or HO_2/RO_x, the other one was from the NO emitted at night with $\Delta^{17}O(NO) \approx 0‰$[76]. Thus NO_2 produced at night was expected to have $\Delta^{17}O(NO_2) = 1/2a\Delta^{17}O(O_3^*)$. In a recent observational study in Grenoble[77], the $\Delta^{17}O(NO_2)$ values showed a large diurnal cycle peaking in the late morning (9:00–12:00) at 39.2‰ and decreasing at night until 20.5‰ at 00:00–5:00. In our calculation, the $\Delta^{17}O(NO_2) = a\Delta^{17}O(O_3^*)$ was used to estimate the formation pathways for the daytime and nighttime samples. As discussed, a great portion of NO_2 produced at night had $\Delta^{17}O(NO_2) = 1/2a\Delta^{17}O(O_3^*)$. However, the $\Delta^{17}O(NO_3^-)$ of the nighttime samples were a lot beyond the range of $\Delta^{17}O(HNO_3)$ of each pathway at night calculated by using $\Delta^{17}O(NO_2) = 1/2a\Delta^{17}O(O_3^*)$ (Supplementary Fig. 6). Since the atmospheric lifetime of NO_x near the surface against nighttime oxidation to nitrate was typically greater than 24 h[13], most nitrate formed during the nighttime would form from NO_2 that reached photochemical equilibrium during the previous day. Consequently, the $\Delta^{17}O(NO_2)$ and the $\Delta^{17}O(HNO_3)$ in each nitrate formation pathway might be overestimated. And the contribution of the pathway that has higher $\Delta^{17}O(NO_3^-)$ ($NO_3 + HC/H_2O$ and N_2O_5 uptake) might be underestimated to varying degrees, especially at night. Despite all the complicated variations of reactions, our results strongly suggested the higher contribution of $NO_2 + OH$ pathway during the day and nocturnal chemistry at night.

As shown in Fig. 3, nocturnal processes contributed the major fractions to nitrate formation on haze days. The average contributions of P1, P2, and P3 were 38, 25, and 36% on haze days, respectively. This result was very different from that during clean days, in which P1, P2, and P3 contributed 47, 21, and 32% to nitrate production, respectively. To understand the diurnal formation mechanisms of nitrate aerosols under different pollution conditions in Nanjing, the fractions of the different pathways to nitrate formation at the different times of the day under clean and haze air conditions are shown in Fig. 5. On clean days (January 14th 2:00 to 16th 8:00), there was no obvious discrepancy in nitrate formation from 5:00 to 20:00, but an apparent difference was found at 23:00–2:00. The average contribution of $NO_2 + OH/H_2O$ oxidation was 50% at 5:00–20:00, dropping to 38% at 23:00–2:00. In contrast, the average contributions of $NO_3 + HC/H_2O$ and $N_2O_5 + Cl^-$ pathway and $N_2O_5 + H_2O$ pathway were 19 and 30% at 5:00–20:00 and increased to 25 and 38% at 23:00–2:00. However, the diurnal variation of nitrate formation on haze days was more obvious than that on clean days. On haze days (January 21st 8:00 to 27th 2:00), the fractions of $NO_2 + OH/H_2O$ pathway to nitrate production gradually increased from 27% at 5:00 to 51% at noon and then decreased with sunset until the lowest (27%) at midnight. Nevertheless, the contribution of $NO_3 + HC/H_2O$ and $N_2O_5 + Cl^-$ pathway decreased with sunrise, which from 40% at 5:00 to the lowest (15%) around noon and increased to 32% at 23:00. The contribution of $N_2O_5 + H_2O$ pathway showed a similar diurnal variation to $NO_3 + HC/H_2O$ and $N_2O_5 + Cl^-$ pathway, but kept a relatively stable level (32–41%) as a whole. The fractions of $NO_3 + HC/H_2O$ and $N_2O_5 + Cl^-/H_2O$ showed a significant positive correlation ($r = 0.81$, $p < 0.01$) with NO_2 concentrations on haze days but no correlation on clean days, suggesting that large emissions of gas precursors like NO*x* might significantly affect the nitrate formation in the haze events. On haze days, the daytime RH values were much lower than those at night, but the fractions of $N_2O_5 + H_2O$ pathway were still at a high level during the day. This suggested the important role of the hydrolysis of N_2O_5 on particle surfaces in nitrate production in the heavily polluted atmosphere even during the daytime.

The effect of air cleaning for resetting the nitrate chemistry

As mentioned above, $\Delta^{17}O(NO_3^-)$ of the 3 h samples were affected by both accumulated nitrate produced prior to the current sampling period and fresh nitrate produced during the current sample period. Fortunately, three precipitation events happened on January 14th, 25th, and 27th during the sampling period (Fig. 2b), eliminating the effect of $\Delta^{17}O(NO_3^-)$ buffering caused by nitrate accumulation. After the precipitation event on January 14th, the concentrations of nitrate and tracer gases (NO_2 and CO) were at the lowest levels (Fig. 2c) during the entire period accompanied with the lower wind speeds until January 16th (Fig. 1c). Therefore, the formation mechanisms quantified by the $\Delta^{17}O(NO_3^-)$ of high-time resolved aerosols after the precipitation were closer to the current nitrate production in the ambient atmosphere. At the beginning of this period, the $\Delta^{17}O(NO_3^-)$ showed low values and averaged at 26.1 ± 1.8‰ from January 14th 2:00 to January 15th 11:00 (Fig. 2a). On average, the $NO_2 + OH$ pathway and $N_2O_5 + H_2O$ pathway contributed 70 ± 10 and 24 ± 8% to nitrate production (Fig. 3), respectively. At the same time, O_3 concentrations remained in a stable level (20 ± 2 ppb) from January 14th 2:00 to January 15th 11:00 (Fig. 2b), which indicated the low NO level after the rainfall limited the reaction of NO with O_3 to form NO_2 and then the photolysis of NO_2 by daylight. Although the contributions of nocturnal pathways ($NO_3 + HC/H_2O$ and $N_2O_5 + H_2O/Cl^-$) showed higher fractions at night than those during the day, the nitrate aerosols collected at night were mainly formed through $NO_2 + OH$ reaction. The low NO_x and atmospheric pollutants (e.g., CO, VOCs) levels in the air after the

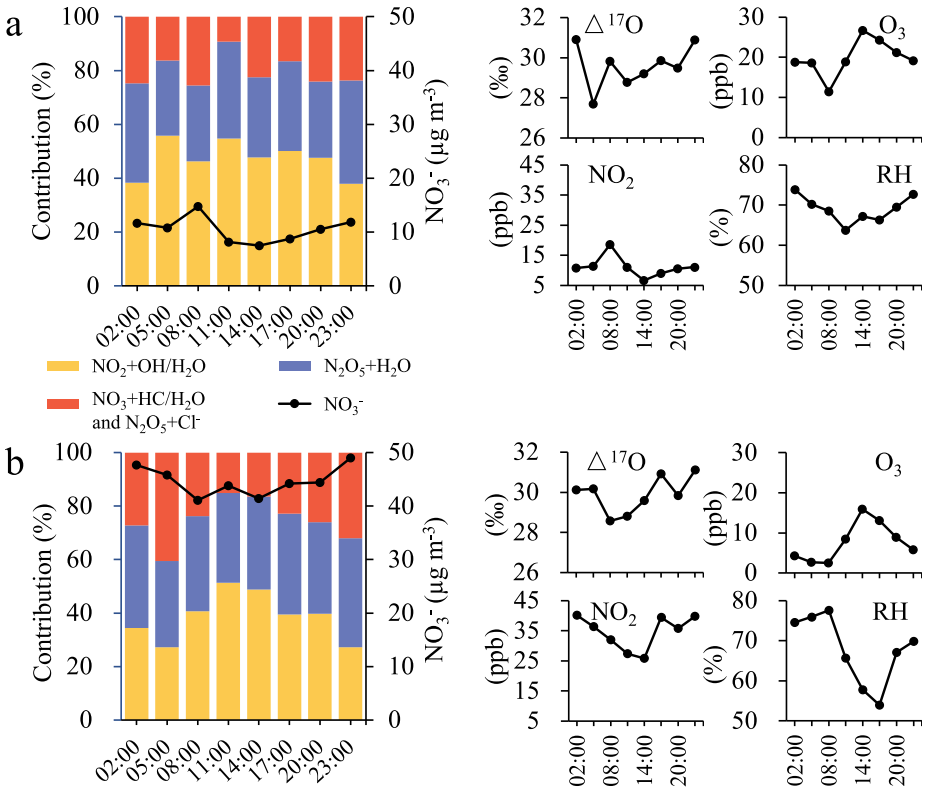

Fig. 5 Diurnal variations of nitrate formation pathways during clean and haze periods. The changes in mass concentrations of nitrate (NO_3^-), the relative contributions of three pathways (pathway 1: $NO_2 + OH/H_2O$, pathway 2: $N_2O_5 + H_2O$ and pathway 3: $NO_3 + HC/H_2O$ and $N_2O_5 + Cl^-$) to nitrate production, oxygen isotope anomaly of nitrate ($\Delta^{17}O(NO_3^-)$), ozone (O_3), nitrogen dioxide (NO_2) and relative humidity (RH) **a** during clean period and **b** during haze period.

precipitation reduced the nitrate production rates through $NO_3 +$ HC and N_2O_5 hydrolysis reactions at night. And some nitrate formed through $NO_2 + OH$ reaction during the day would be collected by the nighttime samples. Interestingly, the $\Delta^{17}O(NO_3^-)$ suddenly increased on January 15th 2:00 and averaged at 33.7 ± 0.9‰ during January 15th 2:00–16th 8:00 (Fig. 2a). The NO_3^-, NO_2, and CO concentrations increased gradually and O_3 began to show significant diurnal variation (Fig. 2). Nocturnal pathways contributed a total of 80% to nitrate formation (Fig. 3). These results suggested that the active photochemical reactions dominated the nitrate production under the strong sunlight in the clean atmosphere and nocturnal chemistry played a key role in the formation of nitrate pollution.

The other case of $\Delta^{17}O(NO_3^-)$ decline occurred before the rain on January 25th. It is notable that both NO_3^- (11 μg m^{-3}) and the $\Delta^{17}O$ (NO_3^-) (~6‰) suddenly decreased after the constant southeast wind turned to the north (Figs. 1c and 2a). The change of wind direction indicated the transport of air masses from the north, which blocked the continuous influence of the original air masses. In this case, we inferred that the decrease of $\Delta^{17}O(NO_3^-)$ before the precipitation resulted from the transport of cleaner air masses and the rainfall continued to scavenge the accumulated nitrate. Therefore, the nitrate collected after the transport of clean air masses and/or the precipitation were mostly newly formed in the atmosphere, the whole system of nitrate chemistry was reset and nitrate accumulation restarted. In other words, $\Delta^{17}O(NO_3^-)$ values after the precipitation were able to reveal the quick variation of nitrate production in the atmosphere. This typical event was affected by the combination of precipitation and the clean air transport, resulting in a rapid decrease of $\Delta^{17}O(NO_3^-)$ (over 10‰ in 15 h) during the severe haze on January 25th. $\Delta^{17}O(NO_3^-)$ was steady around 30–33‰ and suddenly decreased to 23.4‰ after the sunset on January 24th. It showed the minimum value at noon on January 25th and gradually increased back to more than 30‰ after sunset on January 25th (Fig. 2a). Both nitrate and NO_2 showed a similar tendency with $\Delta^{17}O(NO_3^-)$, the accumulated nitrate was effectively washed out by the precipitation[78,79] accompanied with the sudden increase of NOR (from 0.2 to 0.55). This indicated a decreasing fraction of cumulative NO_3^- and an increasing contribution of fresh nitrate with low $\Delta^{17}O(NO_3^-)$ in this precipitation event. The time period before the precipitation went through the most severe haze in the whole sampling period. The low wind speed and stable wind direction (Fig. 1c) suggested that the sampling site was controlled by aged local air masses that moved back and forth in the direction of north and south with consecutive nitrate accumulation since January 23rd. As we illustrated in the previous section, cumulative nitrate has an impact on buffering the $\Delta^{17}O(NO_3^-)$ on haze days. Thus the steady $\Delta^{17}O(NO_3^-)$ before the precipitation and the large contribution of nocturnal formation pathways were observed during the nitrate accumulation in the severe haze (Fig. 3). In addition, HNO_3, N_2O_5, and other soluble species were scavenged by the rain, and NO_2 and CO were much more likely to be diluted by a relatively clean air mass from the north suburb due to the change of wind direction (Fig. 1c). Both the precipitation and the transport of clean air mass helped to reset the whole system of nitrate chemistry. The formation mechanism quantified by the $\Delta^{17}O(NO_3^-)$ of high-time resolved aerosols after this precipitation event also pointed out the dominant contribution of $NO_2 + OH$ to nitrate formation.

Another precipitation event happened on January 27th. In this case, the $\Delta^{17}O(NO_3^-)$ firstly increased after the rainfall during

January 27th 2:00–8:00 and then a largely decline of $\Delta^{17}O(NO_3^-)$ was observed during January 27th 14:00–18:00. The high wind speed and stable wind direction suggested that this sampling period was controlled by transported air masses in the direction of east where some chemical industries located. This meant that although rainfall effectively cleared the air of pollutants, a high value (~36‰) of $\Delta^{17}O(NO_3^-)$ was recorded firstly due to the timely replacement of external nitrates formed by $NO_3 + HC$ pathway. Then NO_3^- and $\Delta^{17}O(NO_3^-)$ rapidly decreased to 3.3 μg m^{-3} and 24.6‰, representing another reset of nitrate chemistry by the rainfall at 14:00 on January 27th. All the three cases discussed above indicated the important role of $NO_2 + OH$ pathway in nitrate production after the air cleaning by precipitation events.

The analysis of diurnal variation of nitrate production based on the $\Delta^{17}O(NO_3^-)$ of high-time-resolved (3 h) aerosols was first conducted during a haze period in Nanjing, a megacity of China. An easy and fast approach was deployed to assess the NO*x* oxidation process, which reduced the inaccuracy of models to the greatest extent with the constraint of $\Delta^{17}O(NO_3^-)$ observation. The effect of nitrate accumulation on buffering the $\Delta^{17}O(NO_3^-)$ on haze days and the cleansing effect for resetting nitrate chemistry was significant for understanding the variation of nitrate production. Thus previous studies of nitrate formation mechanisms based on the daily $\Delta^{17}O(NO_3^-)$ observation might have overestimated the contribution of nocturnal pathways.

Although significantly diurnal variations of nitrate formation pathways based on $\Delta^{17}O(NO_3^-)$ observation were found in this work, we must acknowledge the uncertainties of the diurnal variation on the contribution of nitrate formation pathways due to the absence of the studies on the nighttime NO emissions and NO_2–NO isotope exchange. That requires the enlargement of synchronous studies about triple oxygen isotopes of high-time-resolved atmospheric nitrate and NO/NO_2. Because neither the variation nor the extremum contribution of each pathway could be noticed in lower time-resolved samples such as aerosols collected more than 12 h in previous studies, therefore, it is necessary to study the $\Delta^{17}O(NO_3^-)$ atmospheric nitrate in gas phase and in particles to get a more complete understanding of atmospheric nitrate formation mechanism in future studies.

METHODS

Sampling and atmospheric observation

$PM_{2.5}$ samples were collected from January 14th to 28th, 2015 in Nanjing, China (Supplementary Fig. 7). The sampling site was in the agrometeorological station located on the campus of Nanjing University of Information Science and Technology (32°12'57"N, 118°44'50"E). It was close to a busy road and within the largest industrial complex in Nanjing. Aerosol samples were collected on pre-combusted quartz-fiber filters every 3 h using a high-volume aerosol sampler (KC1000, Qingdao, China) at a flow rate of 1 ± 0.001 m^3 min^{-1}. A field blank was obtained by placing the blank filter on the filter holder for 10 min without pumping. After sampling, all filters were wrapped in aluminum foil, sealed in air-tight polyethylene bags, and stored at −26 °C for later chemical analysis. The details of measurements of pollutant gases, meteorological data, chemical species, and oxygen isotopes of the nitrate are described in the Supporting Information (Supplementary Note 5 and Supplementary Table 2).

Evaluation of nitrate formation mechanism

The observed $\Delta^{17}O(NO_3^-)$ values were used to calculate the contribution of each formation pathway based on isotope mass balance[27]. The $\Delta^{17}O(NO_3^-)$ can be expressed as:

$$\Delta^{17}O(NO_3^-) = \sum \Delta^{17}O(HNO_3)_j \times f_{Pi} \quad (9)$$

where $\Delta^{17}O(NO_3^-)$ was the $\Delta^{17}O$ value of total nitrate, $\Delta^{17}O(HNO_3)_j$ is the $\Delta^{17}O$ value of HNO_3 produced by pathway *j*, f_j is the mole fraction of nitrate produced by *j* HNO_3 formation pathway. Since all the oxygen sources incorporated into nitrate except for O_3, (i.e., water vapor, OH radical, and HO_2 (RO*x*)) were reported to have $\Delta^{17}O \approx 0‰$[34–39]. $\Delta^{17}O(HNO_3)$ value of each pathway can be derived from $\Delta^{17}O(NO_2)$ and written in terms of only $\Delta^{17}O(O_3^*)$ (Eqs. (10)–(12))[80]. $\Delta^{17}O(O_3^*)$ is the $\Delta^{17}O$ value of the terminal oxygen atom of O_3, which transfers to the products during oxidation reactions (Supplementary Table 3)[81]:

$$\Delta^{17}O(HNO_3)_{NO2+OH/H2O} = 2/3a\Delta^{17}O(O_3^*) \quad (10)$$

$$\Delta^{17}O(HNO_3)_{NO3+HC/H2O\ and\ N2O5+Cl-} = 2/3a\Delta^{17}O(O_3^*)+1/3\Delta^{17}O(O_3^*) \quad (11)$$

$$\Delta^{17}O(HNO_3)_{N2O5+H2O} = 2/3a\Delta^{17}O(O_3^*)+1/6\Delta^{17}O(O_3^*) \quad (12)$$

The *a* factor is the mole fraction of NO oxidized by O_3 (Supplementary Note 1). When the NO*x* cycle achieves at the photochemical steady-state, $\Delta^{17}O(NO_2)$ could be expressed as:

$$\Delta^{17}O(NO_2) = a\Delta^{17}O(O_3^*) \quad (13)$$

The *a* factor could be calculated by considering the reaction constants of these three chemical reactions and the concentrations of the corresponding oxidants[19]:

$$a = k_{R1} \times [NO] \times [O_3] / (k_{R1} \times [NO] \times [O_3] + k_{R2} \times [NO] \times [HO_2\cdot] + k_{R3} \times [NO] \times [RO_2\cdot]) \quad (14)$$

where the reaction constants k_{R1}, k_{R2} and k_{R3} are $3.0 \times 10^{-12} \times e^{(-1500/T)}$, $3.5 \times 10^{-12} \times e^{(270/T)}$ and $3.5 \times 10^{-12} \times e^{(270/T)}$ (cm^3 $molecule^{-1}$ s^{-1}) and *T* is the ambient temperature (K)[82,83]. Due to the lack of HO_2 and RO_2 observation, the HO_2 mixing ratios were estimated by the empirical formulas established in an urban city, in which HO_2 was a function of O_3[84]. The RO_2 concentrations were estimated by the HO_2 concentrations multiplying 0.859[85].

$$[HO_2\cdot]/ppt = \exp(5.7747 \times 10^{-2}[O_3](ppb) - 1.7227) \text{ for daytime} \quad (15)$$

$$[HO_2\cdot]/ppt = \exp(7.7234 \times 10^{-2}[O_3](ppb) - 1.6363) \text{ for nighttime} \quad (16)$$

Ozone's terminal atoms are isotopically enriched relative to the central one (isotopic asymmetry)[86–88]. Laboratory experiments[89] suggested that $\Delta^{17}O(O_3^*)$ is linearly correlated with the $\Delta^{17}O$ value of bulk ozone ($\Delta^{17}O(O_3)$) when the $\Delta^{17}O(O_3)$ is in the range of 20–40‰ by:

$$\Delta^{17}O(O_3^*) = 1.5 \times \Delta^{17}O(O_3) \quad (17)$$

Based on the observations of tropospheric O_3[32,33], $\Delta^{17}O(O_3)$ was assumed to average at 26 ± 1‰ in this study, yielding a $\Delta^{17}O(O_3^*)$ value of ~39‰. The calculated *a* values and $\Delta^{17}O(HNO_3)$ in each formation pathway were showed in Supplementary Fig. 4. The endmember values of $\Delta^{17}O(HNO_3)_{NO2+OH/H2O}$, $\Delta^{17}O(HNO_3)_{NO3+HC/H2O\ and\ N2O5+Cl-}$ and $\Delta^{17}O(HNO_3)_{N2O5+H2O}$ were 15.98–25.22‰, 28.98–38.22‰, and 22.48–31.72‰, respectively. Then the contribution of each nitrate formation pathway and the uncertainty in each pathway could be quantified using the Bayesian model (Supplementary Note 4)[21,90].

DATA AVAILABILITY

All the data used in this paper are available from the Open Science Framework (https://osf.io/5d7qy/, https://doi.org/10.17605/OSF.IO/5D7QY).

CODE AVAILABILITY

The codes are available upon request from the corresponding author Yan-Lin Zhang: dryanlinzhang@outlook.com.

Received: 11 November 2021; Accepted: 27 May 2022;
Published online: 21 June 2022

REFERENCES

1. Zhai, S. et al. Control of particulate nitrate air pollution in China. *Nat. Geosci.* **14**, 389–395 (2021).
2. Huang, R.-J. et al. High secondary aerosol contribution to particulate pollution during haze events in China. *Nature* **514**, 218–222 (2014).
3. Michalski, G., Bhattacharya, S. K. & Mase, D. F. *Handbook of Environmental Isotope Geochemistry: Vol I* (Springer, Berlin, Heidelberg, 2012).

4. Browne, E. C. & Cohen, R. C. Effects of biogenic nitrate chemistry on the NO_x lifetime in remote continental regions. *Atmos. Chem. Phys.* **12**, 11917–11932 (2012).
5. Rodhe, H., Dentener, F. & Michael, S. The global distribution of acidifying wet deposition. *Environ. Sci. Technol.* **36**, 4382–4388 (2002).
6. Zhang, Y. et al. A comparative review of inorganic aerosol thermodynamic equilibrium modules: Similarities, differences, and their likely causes. *Atmos. Environ.* **34**, 117–137 (2000).
7. Jacobs, M. I., Burke, W. J. & Elrod, M. J. Kinetics of the reactions of isoprene-derived hydroxynitrates: Gas phase epoxide formation and solution phase hydrolysis. *Atmos. Chem. Phys.* **14**, 8933–8946 (2014).
8. Rindelaub, J. D., McAvey, K. M. & Shepson, P. B. The photochemical production of organic nitrates from α-pinene and loss via acid-dependent particle phase hydrolysis. *Atmos. Environ.* **100**, 193–201 (2015).
9. Seigneur, C., Saxena, P., & Roth, P. M. Computer simulations of the atmospheric chemistry of sulfate and nitrate formation. *Science* **225**, 1028–1030 (1984).
10. Baergen, A. M. & Donaldson, D. J. Photochemical renoxification of nitric acid on real urban grime. *Environ. Sci. Technol.* **47**, 815–820 (2013).
11. Chan, Y.-C. et al. Heterogeneous nitrate production mechanisms in intense haze events in the North China Plain. *J. Geophys. Res. Atmos.* **126**, e2021JD034688 (2021).
12. Xue, C. et al. HONO budget and its role in nitrate formation in the rural North China Plain. *Environ. Sci. Technol.* **54**, 11048–11057 (2020).
13. Alexander, B. et al. Global inorganic nitrate production mechanisms: Comparison of a global model with nitrate isotope observations. *Atmos. Chem. Phys.* **20**, 3859–3877 (2020).
14. Brown, S. S. et al. Budgets for nocturnal VOC oxidation by nitrate radicals aloft during the 2006 Texas Air Quality Study. *J. Geophys. Res. Atmos.* **116**, D24305 (2011).
15. Heintz, F. et al. Long-term observation of nitrate radicals at the Tor Station, Kap Arkona (Rügen). *J. Geophys. Res. Atmos.* **101**, 22891–22910 (1996).
16. Wang, H. et al. Efficient N_2O_5 uptake and NO_3 oxidation in the outflow of urban Beijing. *Atmos. Chem. Phys.* **18**, 9705–9721 (2018).
17. Preunkert, S. et al. Seasonality of sulfur species (dimethyl sulfide, sulfate, and methanesulfonate) in Antarctica: Inland versus coastal regions. *J. Geophys. Res. Atmos.* **113**, D15302 (2008).
18. Thornton, J. A. et al. A large atomic chlorine source inferred from mid-continental reactive nitrogen chemistry. *Nature* **464**, 271–274 (2010).
19. Alexander, B. et al. Quantifying atmospheric nitrate formation pathways based on a global model of the oxygen isotopic composition ($\Delta^{17}O$) of atmospheric nitrate. *Atmos. Chem. Phys.* **9**, 5043–5056 (2009).
20. He, P. et al. Atmospheric $\Delta^{17}O$ (NO_3^-) reveals nocturnal chemistry dominates nitrate production in Beijing haze. *Atmos. Chem. Phys.* **18**, 14465–14476 (2018).
21. Fan, M.-Y. et al. Changes of emission sources to nitrate aerosols in Beijing after the clean air actions: Evidence from dual isotope compositions. *J. Geophys. Res. Atmos.* **125**, e2019JD031998 (2020).
22. Burkholder, J. B. et al. *Chemical Kinetics and Photochemical Data for Use in Atmospheric Studies, Evaluation Number 18* (California Institute of Technology, United States, 2015).
23. Crowley, J. N. et al. Evaluated kinetic and photochemical data for atmospheric chemistry: Volume V – heterogeneous reactions on solid substrates. *Atmos. Chem. Phys.* **10**, 9059–9223 (2010).
24. Tan, F. et al. Heterogeneous reactions of NO_2 with $CaCO_3$–$(NH_4)_2SO_4$ mixtures at different relative humidities. *Atmos. Chem. Phys.* **16**, 8081–8093 (2016).
25. Wang, X. et al. Particulate nitrate formation in a highly polluted urban area: A case study by single-particle mass spectrometry in Shanghai. *Environ. Sci. Technol.* **43**, 3061–3066 (2009).
26. Platt, U. et al. The diurnal variation of NO_3. *J. Geophys. Res. Oceans* **86**, 11965–11970 (1981).
27. Michalski, G. et al. First measurements and modeling of $\Delta^{17}O$ in atmospheric nitrate. *Geophys. Res. Lett.* **30**, 1870 (2003).
28. Matsuhisa, Y., Goldsmith, J. R. & Clayton, R. N. Mechanisms of hydrothermal crystallization of quartz at 250 °C and 15 kbar. *Geochim. Cosmochim. Acta* **42**, 173–182 (1978).
29. Thiemens, M. Mass-independent isotope effects in planetary atmospheres and the early solar system. *Science* **283**, 341–345 (1999).
30. Zhang, W. & Zhang, Y. Oxygen isotope anomaly ($\Delta^{17}O$) in atmospheric nitrate: A review. *Sci. Bull.* **64**, 649–662 (2019).
31. Proemse, B. C. et al. Isotopic characterization of nitrate, ammonium, and sulfate in stack $PM_{2.5}$ emissions in the Athabasca Oil Sands Region, Alberta, Canada. *Atmos. Environ.* **60**, 555–563 (2012).
32. Ishino, S. et al. Seasonal variations of triple oxygen isotopic compositions of atmospheric sulfate, nitrate, and ozone at Dumont d'Urville, coastal Antarctica. *Atmos. Chem. Phys.* **17**, 3713–3727 (2017).
33. Vicars, W. C. & Savarino, J. Quantitative constraints on the ^{17}O-excess ($\Delta^{17}O$) signature of surface ozone: Ambient measurements from 50°N to 50°S using the nitrite-coated filter technique. *Geochim. Cosmochim. Acta* **135**, 270–287 (2014).
34. Barkan, E. & Luz, B. High precision measurements of $^{17}O/^{16}O$ and $^{18}O/^{16}O$ ratios in H_2O. *Rapid Commun. Mass Spectrom.* **19**, 3737–3742 (2005).
35. Luz, B. & Barkan, E. The isotopic ratios $^{17}O/^{16}O$ and $^{18}O/^{16}O$ in molecular oxygen and their significance in biogeochemistry. *Geochim. Cosmochim. Acta* **69**, 1099–1110 (2005).
36. Lyons, J. R. Transfer of mass-independent fractionation in ozone to other oxygen-containing radicals in the atmosphere. *Geophys. Res. Lett.* **28**, 3231–3234 (2001).
37. Meijer, H. A. J. & Li, W. J. The use of electrolysis for accurate $\delta^{17}O$ and $\delta^{18}O$ isotope measurements in water. *Isotopes Environ. Health Stud.* **34**, 349–369 (1998).
38. Morin, S. et al. Signature of Arctic surface ozone depletion events in the isotope anomaly ($\Delta^{17}O$) of atmospheric nitrate. *Atmos. Chem. Phys.* **7**, 1451–1469 (2007).
39. Savarino, J. & Thiemens, M. H. Analytical procedure to determine both $\delta^{18}O$ and $\delta^{17}O$ of H_2O_2 in natural water and first measurements. *Atmos. Environ.* **33**, 3683–3690 (1999).
40. Fan, M.-Y. et al. Important role of NO_3 radical to nitrate formation aloft in urban Beijing: Insights from triple oxygen isotopes measured at the tower. *Environ. Sci. Technol.* https://doi.org/10.1021/acs.est.1c02843 (2021).
41. Lin, Y.-C. et al. Formation mechanisms and source apportionments of airborne nitrate aerosols at a Himalayan-Tibetan Plateau site: Insights from nitrogen and oxygen isotopic compositions. *Environ. Sci. Technol.* **55**, 12261–12271 (2021).
42. Rose, L. A. et al. High resolution, extreme isotopic variability of precipitation nitrate. *Atmos. Environ.* **207**, 63–74 (2019).
43. Wang, Y.-L. et al. Influences of atmospheric pollution on the contributions of major oxidation pathways to $PM_{2.5}$ nitrate formation in Beijing. *J. Geophys. Res. Atmos.* **124**, 4174–4185 (2019).
44. Xie, M. et al. Temporal characterization and regional contribution to O_3 and NO*x* at an urban and a suburban site in Nanjing, China. *Sci. Total Environ.* **551–552**, 533–545 (2016).
45. Ma, X. et al. Winter photochemistry in Beijing: Observation and model simulation of OH and HO_2 radicals at an urban site. *Sci. Total Environ.* **685**, 85–95 (2019).
46. Maji, S., Beig, G. & Yadav, R. Winter VOCs and OVOCs measured with PTR-MS at an urban site of India: Role of emissions, meteorology and photochemical sources. *Environ. Pollut.* **258**, 113651 (2020).
47. Wang, L. et al. Impacts of the near-surface urban boundary layer structure on $PM_{2.5}$ concentrations in Beijing during winter. *Sci. Total Environ.* **669**, 493–504 (2019).
48. Huang, W. et al. Exploring the inorganic and organic nitrate aerosol formation regimes at a suburban site on the North China Plain. *Sci. Total Environ.* **768**, 144538 (2021).
49. Kuang, Y. et al. Explosive morning growth phenomena of NH_3 on the North China Plain: Causes and potential impacts on aerosol formation. *Environ. Pollut.* **257**, 113621 (2020).
50. Tan, Z. et al. An observational based modeling of the surface layer particulate nitrate in the North China Plain during summertime. *J. Geophys. Res. Atmos.* **126**, e2021JD035623 (2021).
51. Liu, P. et al. Formation mechanisms of atmospheric nitrate and sulfate during the winter haze pollution periods in Beijing: gas-phase, heterogeneous and aqueous-phase chemistry. *Atmos. Chem. Phys.* **20**, 4153–4165 (2020).
52. Sun, Y. et al. Chemical characteristics of $PM_{2.5}$ and PM_{10} in Haze−Fog episodes in Beijing. *Environ. Sci. Technol.* **40**, 3148–3155 (2006).
53. Guha, T. et al. Isotopic ratios of nitrate in aerosol samples from Mt. Lulin, a high-altitude station in Central Taiwan. *Atmos. Environ.* **154**, 53–69 (2017).
54. He, P. et al. The observation of isotopic compositions of atmospheric nitrate in Shanghai China and its implication for reactive nitrogen chemistry. *Sci. Total Environ.* **714**, 136727 (2020).
55. Thiemens, M. H. History and appications of mass-independent isotope effects. *Annu Rev. Earth Planet Sci.* **34**, 217–262 (2006).
56. Cristofanelli, P. et al. Tropospheric ozone variations at the Nepal Climate Observatory-Pyramid (Himalayas, 5079 m a.s.l.) and influence of deep stratospheric intrusion events. *Atmos. Chem. Phys.* **10**, 6537–6549 (2010).
57. Savarino, J. et al. Nitrogen and oxygen isotopic constraints on the origin of atmospheric nitrate in coastal Antarctica. *Atmos. Chem. Phys.* **7**, 1925–1945 (2007).
58. McCabe, J. R. et al. A record of ozone variability in South Pole Antarctic snow: Role of nitrate oxygen isotopes. *J. Geophys. Res. Atmos.* **112**, D12303 (2007).
59. Chen, X. R. et al. Field determination of nitrate formation pathway in winter Beijing. *Environ. Sci. Technol.* **54**, 9243–9253 (2020).
60. Ma, Y. et al. How do aerosols above the residual layer affect the planetary boundary layer height? *Sci. Total Environ.* **814**, 151953 (2022).
61. Blay-Carreras, E. et al. Role of the residual layer and large-scale subsidence on the development and evolution of the convective boundary layer. *Atmos. Chem. Phys.* **14**, 4515–4530 (2014).

62. Tsapakis, M. & Stephanou, E. G. Diurnal cycle of PAHs, Nitro-PAHs, and oxy-PAHs in a high oxidation capacity marine background atmosphere. *Environ. Sci. Technol.* **41**, 8011–8017 (2007).
63. Tan, Z. et al. Wintertime photochemistry in Beijing: Observations of RO_x radical concentrations in the North China Plain during the BEST-ONE campaign. *Atmos. Chem. Phys.* **18**, 12391–12411 (2018).
64. Stark, H. et al. Atmospheric in situ measurement of nitrate radical (NO_3) and other photolysis rates using spectroradiometry and filter radiometry. *J. Geophys. Res. Atmos.* **112**, D10S04 (2007).
65. Hellén, H. et al. Long-term measurements of volatile organic compounds highlight the importance of sesquiterpenes for the atmospheric chemistry of a boreal forest. *Atmos. Chem. Phys.* **18**, 13839–13863 (2018).
66. Olson, D. A. et al. Time series analysis of wintertime O_3 and NO_x formation using vector autoregressions. *Atmos. Environ.* **218**, 116988 (2019).
67. Xia, L. et al. Source apportionment of VOCs in a suburb of Nanjing, China, in autumn and winter. *J. Atmos. Chem.* **71**, 175–193 (2014).
68. Walker, H. M. et al. Night-time measurements of HO_x during the RONOCO project and analysis of the sources of HO_2. *Atmos. Chem. Phys.* **15**, 8179–8200 (2015).
69. Paulson, S. E. & Orlando, J. J. The reactions of ozone with alkenes: An important source of HO_x in the boundary layer. *Geophys. Res. Lett.* **23**, 3727–3730 (1996).
70. Emmerson, K., Carslaw, N. & Pilling, M. Urban atmospheric chemistry during the PUMA campaign 2: Radical budgets for OH, HO_2, and RO_2. *J. Atmos. Sci.* **52**, 165–183 (2005).
71. Lowe, D. et al. WRF-Chem model predictions of the regional impacts of N_2O_5 heterogeneous processes on night-time chemistry over north-western Europe. *Atmos. Chem. Phys.* **15**, 1385–1409 (2015).
72. Wang, H. et al. NO_3 and N_2O_5 chemistry at a suburban site during the EXPLORE-YRD campaign in 2018. *Atmos. Environ.* **224**, 117180 (2020).
73. Liu, L. et al. Wintertime nitrate formation pathways in the north China plain: Importance of N_2O_5 heterogeneous hydrolysis. *Environ. Pollut.* **266**, 115287 (2020).
74. Park, R. J. et al. Natural and transboundary pollution influences on sulfate-nitrate-ammonium aerosols in the United States: Implications for policy. *J. Geophys. Res. Atmos.* **109**, D15204 (2004).
75. Walters, W. W. & Michalski, G. Theoretical calculation of oxygen equilibrium isotope fractionation factors involving various NOy molecules, OH, and H_2O and its implications for isotope variations in atmospheric nitrate. *Geochim. Cosmochim. Acta* **191**, 89–101 (2016).
76. Zhang, S. et al. High-resolution simulation of link-level vehicle emissions and concentrations for air pollutants in a traffic-populated eastern Asian city. *Atmos. Chem. Phys.* **16**, 9965–9981 (2016).
77. Albertin, S. et al. Measurement report: Nitrogen isotopes ($\delta^{15}N$) and first quantification of oxygen isotope anomalies ($\Delta^{17}O$, $\delta^{18}O$) in atmospheric nitrogen dioxide. *Atmos. Chem. Phys.* **21**, 10477–10497 (2021).
78. Morin, S. et al. Comprehensive isotopic composition of atmospheric nitrate in the Atlantic Ocean boundary layer from 65°S to 79°N. *J. Geophys. Res. Atmos.* **114**, D05303 (2009).
79. Fang, Y. T. et al. Anthropogenic imprints on nitrogen and oxygen isotopic composition of precipitation nitrate in a nitrogen-polluted city in southern China. *Atmos. Chem. Phys.* **11**, 1313–1325 (2011).
80. Savarino, J. et al. Oxygen isotope mass balance of atmospheric nitrate at Dome C, East Antarctica, during the OPALE campaign. *Atmos. Chem. Phys.* **16**, 2659–2673 (2016).
81. Savarino, J. et al. The $NO+O_3$ reaction: A triple oxygen isotope perspective on the reaction dynamics and atmospheric implications for the transfer of the ozone isotope anomaly. *J. Chem. Phys.* **128**, 194303 (2008).
82. Kunasek, S. A. et al. Measurements and modeling of $\Delta^{17}O$ of nitrate in snowpits from Summit, Greenland. *J. Geophys. Res. Atmos.* **113**, D24302 (2008).
83. Sander, S. et al. *Chemical Kinetics and Photochemical Data for Use in Atmospheric Studies, Evaluation Number 14* (California Institute of Technology, United States, 2011).
84. Kanaya, Y. et al. Urban photochemistry in central Tokyo: 1. Observed and modeled OH and HO_2 radical concentrations during the winter and summer of 2004. *J. Geophys. Res. Atmos.* **112**, D21312 (2007).
85. Liu, Z. et al. Summertime photochemistry during CARE Beijing-2007: RO_x budgets and O_3 formation. *Atmos. Chem. Phys.* **12**, 7737–7752 (2012).
86. Anderson, S. M., Morton, J. & Mauersberger, K. Laboratory measurements of ozone isotopomers by tunable diode laser absorption spectroscopy. *Chem. Phys. Lett.* **156**, 175–180 (1989).
87. Janssen, C. Intramolecular isotope distribution in heavy ozone ($^{16}O^{18}O^{16}O$ and $^{16}O^{16}O^{18}O$). *J. Geophys. Res. Atmos.* **110**, D08308 (2005).
88. Michalski, G., Bhattacharya, S. K. & Thiemens, M. H. The role of symmetry in the mass independent isotope effect in ozone. *Proc. Natl Acad. Sci. USA* **106**, 5493–5496 (2009).
89. Vicars, W. C. et al. Measurement of the 17O-excess ($\Delta^{17}O$) of tropospheric ozone using a nitrite-coated filter. *Rapid Commun. Mass Spectrom.* **26**, 1219–1231 (2012).
90. Parnell, A. C. et al. Bayesian stable isotope mixing models. *Environmetrics* **24**, 387–399 (2013).

ACKNOWLEDGEMENTS

This study is supported by the National Natural Science Foundation of China (grant nos. 42192512 and 41977305) and the National Key Research and Development Program of China (grant no. 2017YFC0212704).

AUTHOR CONTRIBUTIONS

Y.-L.Z. designed the experiments. W.Z., M.-Y.F., J.L., Y.-L.Z., and G.M. conceived and organized this paper. W.Z., X.L., F.C., and M.B. conducted the aerosol collection and the measurements of meteorological parameters. W.Z., H.F., J.L., and B.P.W. conducted the measurement of triple oxygen isotopes, Y.H. run the FLEXPART model, M.-Y.F. and Y.-L.Z. prepared the manuscript with contributions from all co-authors.

COMPETING INTERESTS

The authors declare no competing interests.

ADDITIONAL INFORMATION

Supplementary information The online version contains supplementary material available at https://doi.org/10.1038/s41612-022-00273-3.

Correspondence and requests for materials should be addressed to Yan-Lin Zhang.

Reprints and permission information is available at http://www.nature.com/reprints

Publisher's note Springer Nature remains neutral with regard to jurisdictional claims in published maps and institutional affiliations.